

Full length article

High-pressure torsion driven phase transformations in Cu–Al–Ni shape memory alloys



B.B. Straumal^{a, b, c, *}, A.R. Kilmametov^{a, d}, G.A. López^e, I. López-Ferreño^f, M.L. Nó^e, J. San Juan^f, H. Hahn^a, B. Baretzky^a

^a Karlsruhe Institute of Technology, Institute of Nanotechnology, 76344 Eggenstein-Leopoldshafen, Germany

^b Institute of Solid State Physics, Russian Academy of Sciences, 142432 Chernogolovka, Russia

^c National University of Science and Technology «MISIS», Leninskii prosp. 4, 119049 Moscow, Russia

^d Institute of Physics of Advanced Materials, Ufa State Aviation Technical University, K. Marx St. 12, 450000 Ufa, Russia

^e Applied Physics II, University of the Basque Country UPV-EHU, Apdo. 644, 48080 Bilbao, Spain

^f Condensed Matter Physics, University of the Basque Country UPV-EHU, Apdo. 644, 48080 Bilbao, Spain

ARTICLE INFO

Article history:

Received 15 October 2016

Received in revised form

3 December 2016

Accepted 4 December 2016

Keywords:

High-pressure torsion

Precipitation

Decomposition

Phase transitions

Shape memory alloys

ABSTRACT

Severe plastic deformation (SPD) frequently induces phase transformations like decomposition of supersaturated solid solution, dissolution of precipitates, amorphization, nanocrystallization etc. Such diffusive phase transitions are combined with SPD-driven accelerated mass transfer. Displacive (or martensitic) phase transitions can also take place and in combination with diffusive ones have not been investigated in depth in severely deformed materials. The goal of this work is to investigate the combination of displacive (austenite ↔ martensite) and diffusive (decomposition of supersaturated solid solution) phase transitions in two different Cu–Al–Ni shape memory alloys under the influence of high-pressure torsion (HPT). After homogenization in the one-phase (austenitic) β -area of Cu–Al–Ni phase diagram and quenching, the first alloy was in martensitic state (mainly β'_3 martensite with a small amount of γ'_3 martensite), and the second one remained austenitic (β_3 phase). The HPT of these alloys led to the precipitation of α_1 -phase in the first case and γ_1 -phase in the second one (as if they were annealed at an effective temperature $T_{\text{eff}} = 620 \pm 20$ °C). As a result of precipitation, the matrix in the first alloy was enriched and in the second one depleted in Al. After HPT, both alloys contained mainly β'_3 martensite with a certain amount of γ'_3 martensite. Thus, the HPT-driven diffusive transformations (precipitation of α_1 - and γ_1 -phase) influence the followed displacive (martensitic) transformation. Simultaneously, a dramatic grain refinement is obtained and the reported results open new possibilities to investigate the superelastic and shape memory effects in nanostructured Cu–Al–Ni alloys.

© 2016 Acta Materialia Inc. Published by Elsevier Ltd. All rights reserved.

1. Introduction

Severe plastic deformation (SPD) frequently induces phase transformations [1] like formation [2–4] or decomposition of supersaturated solid solution [5–9], dissolution of precipitates [10–15], amorphization [16–21], nanocrystallization [22–24] etc. In some cases such transitions proceed simultaneously and compete with each other [8,25]. All these transitions are diffusive, i.e. they need the long-range redistribution of different components in an alloy. Such phase transformations under SPD are usually

combined with SPD-driven accelerated mass transfer. The acceleration of diffusion takes place due to the formation and annihilation (in dynamic equilibrium) of huge amount of vacancies and other lattice defects during SPD [25]. In addition to the diffusive phase transitions, another class of phase transformations exists, the so-called displacive (or martensitic) transformations. They do not need the long-range mass transfer and involve only the short displacements of atoms. In the last decades some works have been devoted to the investigation of this type of transformations in severely deformed materials such as steels [26] or Ti–Ni-based alloys [17,27–29], among others. However, the combination of both displacive and diffusive phase transitions in the same severely deformed material has not been discussed in depth. In the current work, due to reasons that will be disclosed in the next paragraphs,

* Corresponding author. Institute of Solid State Physics, Russian Academy of Sciences, Chernogolovka, Moscow District, 142432, Russia.

E-mail address: straumal@issp.ac.ru (B.B. Straumal).

such an investigation in Cu–Al–Ni shape memory alloys (SMA) is undertaken. The goal of this work is to investigate the combination of displacive (austenite ↔ martensite) and diffusive (decomposition of supersaturated solid solution) phase transitions under the influence of high-pressure torsion (HPT) in two different Cu–Al–Ni shape memory alloys (SMA).

Shape memory alloys have the ability to recall their previous shape when subjected to certain stimuli such as thermo-mechanical variations. They have attracted considerable attention and interest in a broad range of technological applications, due to their unique properties. A reversible diffusionless phase transition, known as thermoelastic martensitic transformation, is responsible for these characteristics [30–32]. It is known that martensitic transformation occurs between a high-temperature high-symmetry phase called austenite, and a low-temperature low-symmetry phase called martensite. Starting with the early pioneering works, in the 1960's, followed by a strong progress on the first Ti–Ni, the first worldwide known SMA, this type of materials have been developed quite drastically. This progress was summarized in the 1990's [30–32] and more recently revisited in general (fundamentals and applications) [33–37] or with more focused on specific topics such as biomedical applications [38,39], modeling and simulations [40,41] or thin films and micro-electromechanical system (MEMS) applications [42–44]. Cu-based alloys, in particular Cu–Al–Ni ones, are being developed as an alternative to the more widespread Ti–Ni binary SMAs, because they can exhibit better properties like higher transformation temperatures, a large superelastic window, a small thermal hysteresis as well as a high damping coefficient [30–32]. Furthermore, some years ago it has also been demonstrated that the superelastic and shape memory effects occur and are very competitive (large work output, stability upon cycling, etc.) in these ternary alloys also occur at micro- and nano-scale, being an advantage over the Ti–Ni SMAs [45–47].

Nevertheless, as usually happens, some drawbacks exist. The main one is brittleness in conventional polycrystalline state due to their high elastic anisotropy, their large grain size (in as-cast state), and large dependence of the transformation strain on the crystal-line orientation [32], which generate stresses in the grain boundaries and triple junctions [48]. Until now, two rather contrary ways exist in order to overcome this problem: use of single crystals or reduction of the grain size. Grain refinement reduces stress concentration and has been used to improve the mechanical properties of polycrystalline Cu–Al–Ni alloys [49–55]. Particularly, using powder metallurgy for Cu–Al–Ni alloys leads to the reduction of grain size and enhancements of both ductility and shape memory behaviour [52,54,55]. However, further reduction of the grain size is still required in order to obtain more favourable properties.

SPD techniques are very promising for the improvement of the microstructure and properties of Cu-based SMAs by reducing the grain size and have been widely used in different types of materials [57–61]. Among them high-pressure torsion is a well-established SPD procedure for obtaining nanometer- and submicrometer-sized grains and microstructures and even amorphous phases in bulk materials. Furthermore, as mentioned above, it has been reported that HPT can lead to both diffusive [1,9] and displacive (diffusionless) phase transformations [17,27–29] in different materials. Concerning the application of this SPD technique on SMAs, it has already been reported in the literature for Ti–Ni alloys [17,27,28,62–64], but, to our best knowledge, this is not the case for Cu-based SMAs. In this scenario, the feasibility of applying HPT to obtain refined microstructures in Cu-based SMAs deserves to be investigated being the main goal of the present work. A detailed explanation of the combination of SPD-driven diffusive and displacive phase transformations is proposed and this would be the basis for improving the ultimate properties of these materials.

2. Experimental

Two Cu–Al–Ni SMAs (Cu–13.1 wt% Al–3.8 wt% Ni called further as Alloy A and Cu–14.4 wt% Al–4.3 wt% Ni, Alloy B) with slightly different composition and, consequently, different transformation temperatures were selected based on the results of previous works done using single crystals [56,65]. The concentrations of Al and Ni given above were measured using Inductively Coupled Plasma Optical Emission Spectroscopy (ICP-OES). No argon was found in the composition of alloys after hot isostatic pressing (HIP), compaction and hot rolling. Initial pure components (99.99% Cu, 99.99% Al and 99.97% Ni) were pre-alloyed in an Ar atmosphere and subsequently atomized by Ar at 2.3 MPa using a Leybold Viga 2S vertical atomizer to obtain the Cu–Al–Ni SMA powders (particle size fraction used 25–50 μm) (Fig. 1a). HIP at 850 °C, 140 GPa for 2 h in an ABB Autoclave Systems Inc. QIH-3 device was then applied to compact the SMAs powders. The overall microstructure of a compacted sample is shown in Fig. 1b, where the original borders of the starting powder particles surrounded by a thin oxide layer are visible. Afterwards, the alloys were hot-rolled at 850 °C with a thickness reduction of 2% per step down to a thickness of about 0.8 mm (Fig. 1c). Due to this hot-rolling and subsequent slow cooling down to room temperature precipitation of stable phases takes place (grey particles in Fig. 1c, the microstructure is explained in more details in the first paragraph of Results Section). For more details on the alloy production see Refs. [54,55]. Finally, the hot-rolled alloys were homogenized at 900 °C, 0.5 h in Ar and quenched in cold water (at 0 °C). As a result, sample A is in martensite state at room temperature (Fig. 1d), whereas sample B is in austenite state (Fig. 1e). The transformation cycles, obtained by integration of the differential scanning calorimetry (DSC) thermograms, are shown for both alloys in Fig. 1f.

For HPT processing, 0.6-mm thick discs with diameter of 10 mm were cut using spark erosion. The samples were subjected to HPT at room temperature, of about 25 °C, under a pressure of 5 GPa in a Bridgman anvil-type unit (5 rotations of the anvil at a rate of 1 rpm) using a custom-built computer controlled HPT device (W. Klement GmbH, Lang, Austria). The torsion torque measured during HPT increased during 1–2 anvil rotations and then remained unchanged (i.e. reached a steady state as in Refs. [7–9,66–69]) in the range of (100 ± 30) H·m, that is a typical value for HPT of Cu-based alloys [8]. The cold working in the HPT machine leads to slight heating of a sample up to about 40–50 °C in the steady state. Samples for microstructural and X-rays investigations were cut from the HPT-processed discs at a distance of 3 mm from the sample center. X-ray diffraction (XRD) patterns were obtained using Bragg–Brentano geometry in a powder diffractometer (Philips X'Pert) with Cu-K α radiation. Lattice parameter values were estimated using the powder diffraction tool of “Fityk” software [70,71]. The initial inspection of the obtained materials was carried out using a Philips XL30 scanning electron microscope (SEM) equipped with an Oxford Instruments LINK ISIS energy-dispersive X-ray spectrometer (EDS). Jeol JSM 6400/7000 F microscopes equipped with Oxford Instruments LINK ISIS EDS spectrometers was also used. The details of the phase composition and crystal structure were investigated by transmission electron microscopy (TEM) using a Philips CM200 microscope equipped with a LaB₆ filament, a super-twin lens and an EDAX EDS system. The operating voltage was 200 kV. Bright field images and electron diffraction patterns (both modes selected area (SAED) and microdiffraction (MD)) were acquired using a CCD camera (TVIPS GmbH). A Philips Be double-tilt holder was used to orient the sample. Electron transparent lamellae were prepared by focused ion beam (FIB) standard methods using a FEI Helios NanoLab Dual Beam 650 equipment.

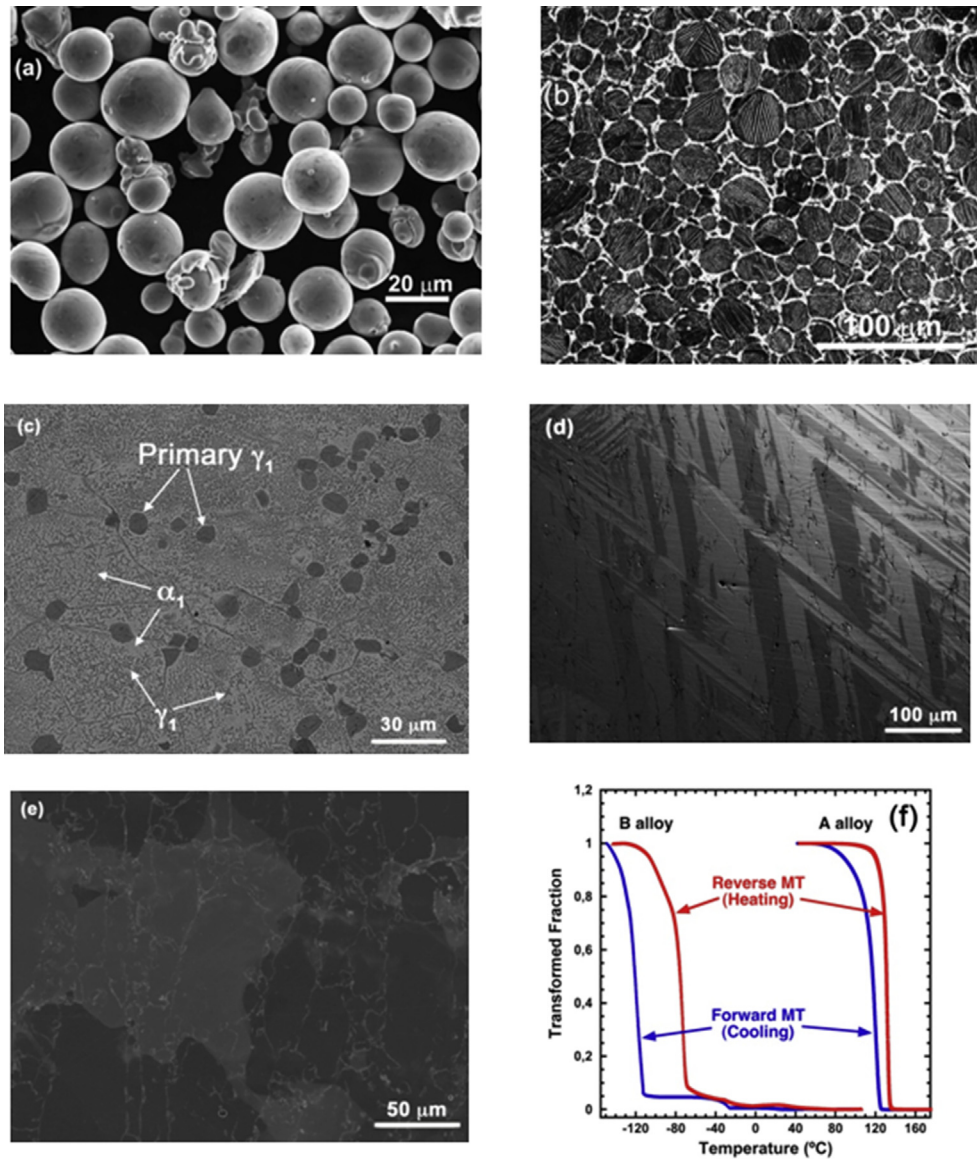


Fig. 1. (a) Secondary electron image of Cu–Al–Ni SMA powders after Ar-atomization. (b) and (c) Back-scattered electron images after HIP at 850 °C and 140 GPa for 2 h, and after hot-rolling at 850 °C, respectively. (d) Optical microscopy image acquired using polarized light of a Cu–13.1 wt% Al–3.8 wt% Ni alloy (A) after annealing at 900 °C for 0.5 h in Ar and subsequent quenching in cold water at 0 °C. (e) Back-scattered electron image of a Cu–14.4 wt% Al–4.3 wt% Ni alloy (B) after annealing at 900 °C for 0.5 h in Ar and subsequent quenching in cold water at 0 °C. (f) Transformation cycles as determined by DSC for alloys A and B.

The identification of the electron diffraction patterns was performed using the Carine program.

3. Results

The microstructures that appeared during the whole material production will be presented very briefly. On average the grain size inside the powder particles after atomization was 10–20 μm (Fig. 1a), although in many cases reach the particle size [55]. After HIP compaction a noticeable grain growth up to 50 μm was observed (Fig. 1b). Upon hot-rolling the microstructure evolved and α_1 and γ_1 stable phases were formed (Fig. 1c). In this sample, since sample B has a hypereutectoid composition, firstly primary proeutectoid γ_1 precipitates (dark equiaxed particles in Fig. 1c) appear, and then the eutectoid decomposition takes place (star-like γ_1 precipitates in the α_1 matrix in Fig. 1c) [72,73]. Finally, after the homogenization and subsequent quenching different types of

microstructure were created. In the alloy with lower content of Al (alloy A), complete martensite transformation evidently occurred, and the size of martensite plates exceeded 100 μm (Fig. 1d). The grain size in the parent austenite phase before the martensitic transformation was between 100 and 500 μm. It is worth to note that oxides particles from the films of the starting powder particles remain in the samples even after hot rolling; and resemble the original particles (initially spherical and then elongated due to rolling), but the grain size of the parent austenite phase is significantly larger than the starting particle size. In the case of the alloy with higher content of Al (alloy B), a coarse-grained structure developed without martensite plates and with rather wide grain size distribution between 20 and 500 μm (Fig. 1e).

The XRD patterns of samples before and after HPT are shown in Fig. 2. It can be clearly seen that after homogenization and subsequent quenching the phases α_1 and γ_1 present in the microstructure after HIP disappeared. Before HPT the Cu–13.1 wt% Al–3.8 wt%

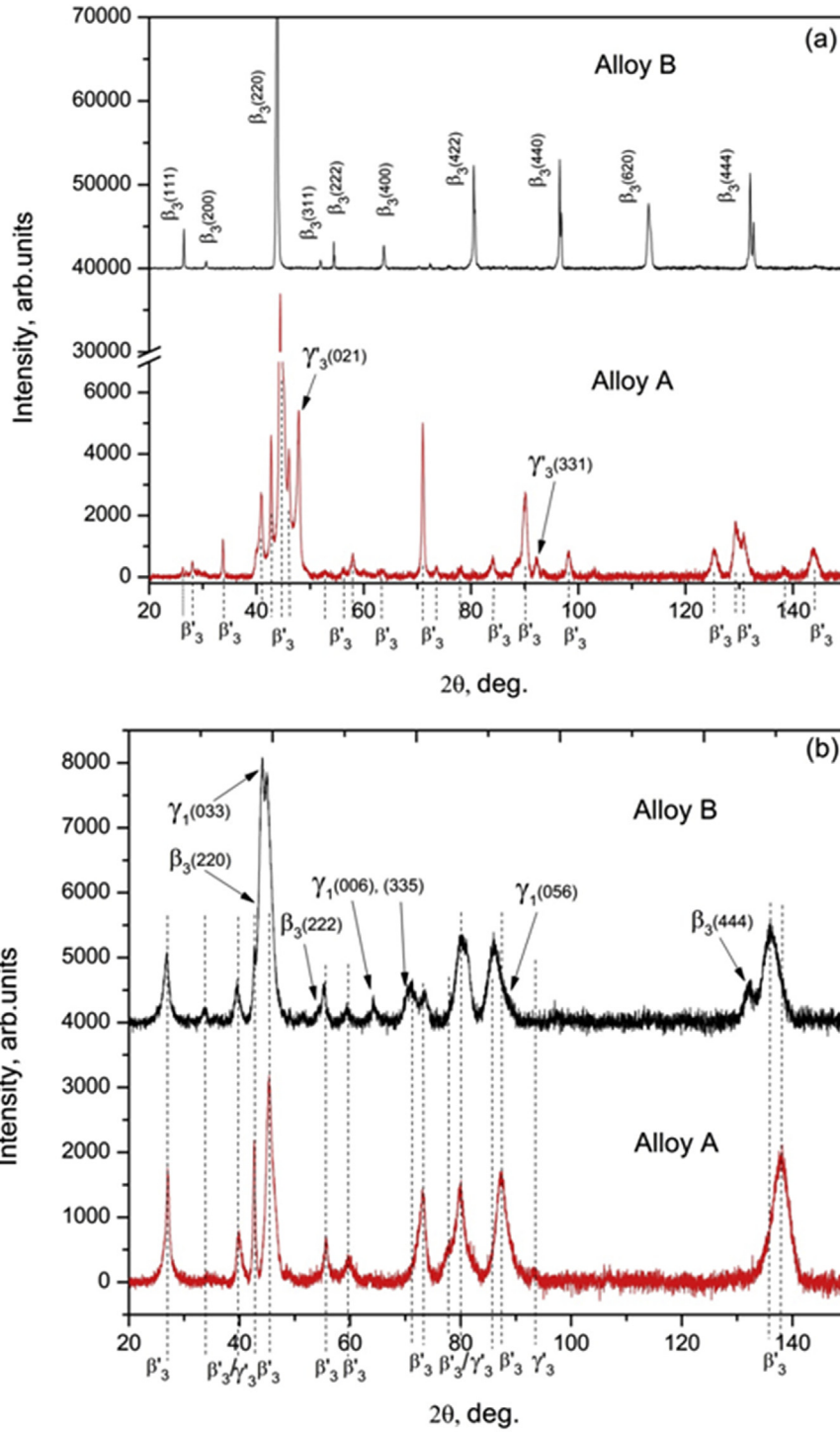


Fig. 2. XRD patterns of Cu–13.1 wt% Al–3.8 wt% Ni (A) and Cu–14.4 wt% Al–4.3 wt% Ni (B) alloys before (a) and after (b) HPT. The positions of numerous β_3 martensite peaks are marked with dotted lines and lettering under the horizontal 2θ axis.

Ni alloy (A) contained two martensitic phases (Fig. 2a, lower curve), i.e. mainly the monoclinic β_3 (C2/m) phase with lattice parameters $a = 1.38043$ nm, $b = 0.52871$ nm, $c = 0.43920$ nm [74] and a small amount of the orthorhombic γ_3 (Pmmn) with lattice parameters $a = 0.55034$ nm, $b = 0.42317$ nm, $c = 0.43562$ nm [75]. The positions of numerous β_3 peaks are marked with dotted lines and lettering under the horizontal 2θ axis. The Cu–14.4 wt% Al–4.3 wt% Ni alloy (B) was in the austenitic state (Fig. 2a, upper curve) and

contained only β_3 phase (highly-ordered cubic phase with L2₁ superstructure and lattice parameter $a = 0.584001$ nm [76]).

For both alloys, HPT led to a high dislocation density in ultra-fine grained microstructure with the typical grain size of 100–300 nm similar to other Cu-based alloys previously processed by this technique [78,67,77–79]. This can be distinctly revealed from the substantial broadening of XRD peaks after HPT (Fig. 2b) in comparison to the initial states of Cu–Al–Ni alloys (Fig. 2a). So, the peak

width at half maximum attained the value of about 2–3° after HPT. Of course, substantial peak broadening takes place not only due to the grain refinement, but it also indicates the high dislocation contents providing a distribution of lattice spacing.

The XRD patterns for both alloys after HPT contain mainly the peaks corresponding to the monoclinic β'_3 (C2/m) martensite which could be indexed with lattice parameters $a = 1.37653$ nm, $b = 0.53883$ nm, $c = 0.43847$ nm in the Cu–13.1 wt% Al–3.8 wt% Ni (A) alloy, and with lattice parameters $a = 1.38674$ nm, $b = 0.52857$ nm, $c = 0.43950$ nm in the Cu–14.4 wt% Al–4.3 wt% Ni (B) alloy, respectively. The alteration in Cu–Al–Ni composition of the alloys, i.e. higher content of Al and Ni atoms in the case of alloy B, produces a change in lattice parameters and consequently causes some shift in XRD peak positions, especially for higher diffraction angles (Fig. 2b). The presence of some small peaks also indicates a certain amount of the orthorhombic γ'_3 (Pmmn) martensite in alloy A, however a strong overlapping of the main peaks attributed to both β'_3 and γ'_3 martensites does not allow to estimate precisely its content. At the same time, XRD pattern of the alloy B subjected to HPT reveals considerable transformation of the structure. Besides martensite β'_3 phase the evident occurrence of the γ_1 (P-43 m) phase [80] with lattice parameter $a = 0.87269$ nm and the presence of a certain amount of parent β_3 austenite can be observed (see upper diffractogram in Fig. 2b). It should be noted that a number of strong peaks of β_3 austenite phase completely disappear after HPT, an only few β_3 peaks remained. This fact indicates that austenite-martensite transformation in alloy B appeared to be not completed. However, similar redistribution of the XRD intensities for both alloys A and B exhibits the development of specific HPT-induced texture that takes place in Cu–Al–Ni β'_3 -martensite under deformation influence.

To complete the bulk information obtained from the XRD, the samples were investigated at a local level using TEM. Fig. 3 shows TEM bright field images and electron diffraction patterns acquired from a TEM lamella of the Cu–14.4 wt% Al–4.3 wt% Ni alloy (B) after HPT. However, it is observed that the original highly-ordered β_3 cubic phase decomposed into a duplex microstructure consisting of precipitates of the stable γ_1 phase homogeneously distributed in a matrix (Fig. 3a). The size of γ_1 precipitates is approximately 50–100 nm, and the size of grains in the matrix is estimated to be about 200–300 nm. More precise measurement of grain size was difficult due to simultaneous presence of austenite and martensite in the sample, as shown in Fig. 3b. According to semi-quantitative (standardless) EDS analysis, the Al content in the γ_1 precipitates was about 23% higher on average than that of the matrix (14.4 wt%) as determined from 8 independent measurements (4 in precipitates and 4 in the matrix). The Ni content is the same in both, precipitates and matrix. It means that after precipitation, which took place during HPT, the matrix has a lower Al content than before HPT. It has also been observed that some areas are in austenite state (see indication in Fig. 3b and the corresponding electron diffraction pattern), therefore, it can be said that the matrix is partly transformed into martensite. This is in agreement with the XRD data (see Fig. 2b upper curve). As an example a SAED pattern corresponding to an austenite grain is shown in Fig. 3c. In the case of the stable γ_1 phase, a pattern was acquired in micro-diffraction mode (MD) (Fig. 3d). In MD mode a nearly parallel focused beam is used to obtain the pattern. This mode is especially suitable to study small precipitates. Concerning the martensite variants or grains, mainly MD patterns corresponding to the monoclinic β'_3 martensite were acquired (Fig. 3e). However, in some cases, streaks along the basal plane of the β'_3 martensite were observed. This is shown in Fig. 3f with MD pattern and additional scheme of the overlapping the simulated patterns for β'_3 and γ'_3 martensitic phases with an experimental one; crosses and circles

correspond to β'_3 martensite and γ'_3 martensite, respectively.

The MD patterns in Fig. 3e and f indicate a faulty structure, which leads to a stacking that could also be indexed using the structure corresponding to the orthorhombic γ'_3 martensite, see the overlapping of the simulated patterns (crosses and circles correspond to β'_3 martensite and γ'_3 martensite, respectively. Scheme is shown below the Fig. 3f) and the experimental ones. In some cases, by using a very small spot size in MD mode, patterns that match well with those of the γ'_3 martensite were acquired (Fig. 3g). Just to better evidence the faulty structure of the martensite variants an enlargement is presented in the bright field image shown in Fig. 3h. The observed microstructure is consistent with a faulty structure, i.e. these are faults. The diffuse scattering observed in Fig. 3e and f (also in Fig. 4e), can only be described crystallographically in terms of stacking faults introduced in the β'_3 martensite structure. It is considered here that these stacking faults appeared due to HPT deformation. After successive deformation these faults end up in very small domains (“nano variants”), whose electron diffraction patterns match well the structure of γ'_3 martensite (Fig. 3g), in agreement with similar reported observations [81]. Just to remind, a twin boundary consists of a mirror plane with the same crystallographic structure at both sides. Understanding the observed microstructure as “internal twins” or micro/nano twins would lead to sharp spots in the electron diffraction patterns, which is not the case.

At this point the TEM bright field images and electron diffraction patterns acquired for the Cu–13.1 wt% Al–3.8 wt% Ni alloy (A) after HPT will be presented (Fig. 4). The microstructure consists mainly of martensite; no austenite was detected. In addition, some small precipitates of the stable α_1 phase were detected. The size of the α_1 precipitates is about 40–60 nm (Fig. 4a) and the grain size in the matrix is about 100–300 nm (Fig. 4b). The semi-quantitative EDS analysis shows that, in accordance with the phase diagram (Fig. 5), the α_1 precipitates contain 12 wt% Al smaller on average than in the matrix (13.1 wt% Al) as determined from 12 independent measurements; 6 in precipitates and 6 in the matrix. The Ni content is the same both in the precipitates and in the matrix. Fig. 4c shows an example of SAED pattern corresponding to the α_1 -phase precipitate. Concerning the structure of the martensitic matrix, SAED and MD patterns corresponding to the monoclinic β'_3 martensite were acquired (Fig. 4d and e). In several cases, streaks along the basal plane of the β'_3 martensite were observed (Fig. 4e). This indicates a faulty structure, which leads to a stacking that can also be indexed using the structure of the γ'_3 martensite, as also observed in sample B. For sample A, several patterns that fit well with those of the orthorhombic γ'_3 martensite were acquired (Fig. 4e). Again, by using a very small spot size, MD patterns that match well with those of the γ'_3 martensite were acquired (Fig. 4f). This amount of γ'_3 martensite can also be understood if we consider that in Cu-based SMA compressive stresses promote preferentially the nucleation of γ'_3 martensite with respect the β'_3 martensite [82]. Analogously as with alloy B, an additional bright field image of the faulty martensites is shown in Fig. 4g.

4. Discussion

Concerning the grain refinement, the achieved ultrafine grain size (100–300 nm, see Figs. 3a and 4a) in both alloys A and B after applying HPT agrees well with previous works on SPD of Cu and Cu-based alloys [7,8,67,68,77–79]. Indeed, in Ref. [77] the grain size in pure Cu after HPT (5 rotations at 6 GPa) measured by TEM was between 100 and 300 nm. Another research group, also observed by TEM a similar grain size in pure Cu processed by HPT (200–300 nm) [78], and they found that XRD of the same samples gave the crystallite size (or the size of coherently scattering

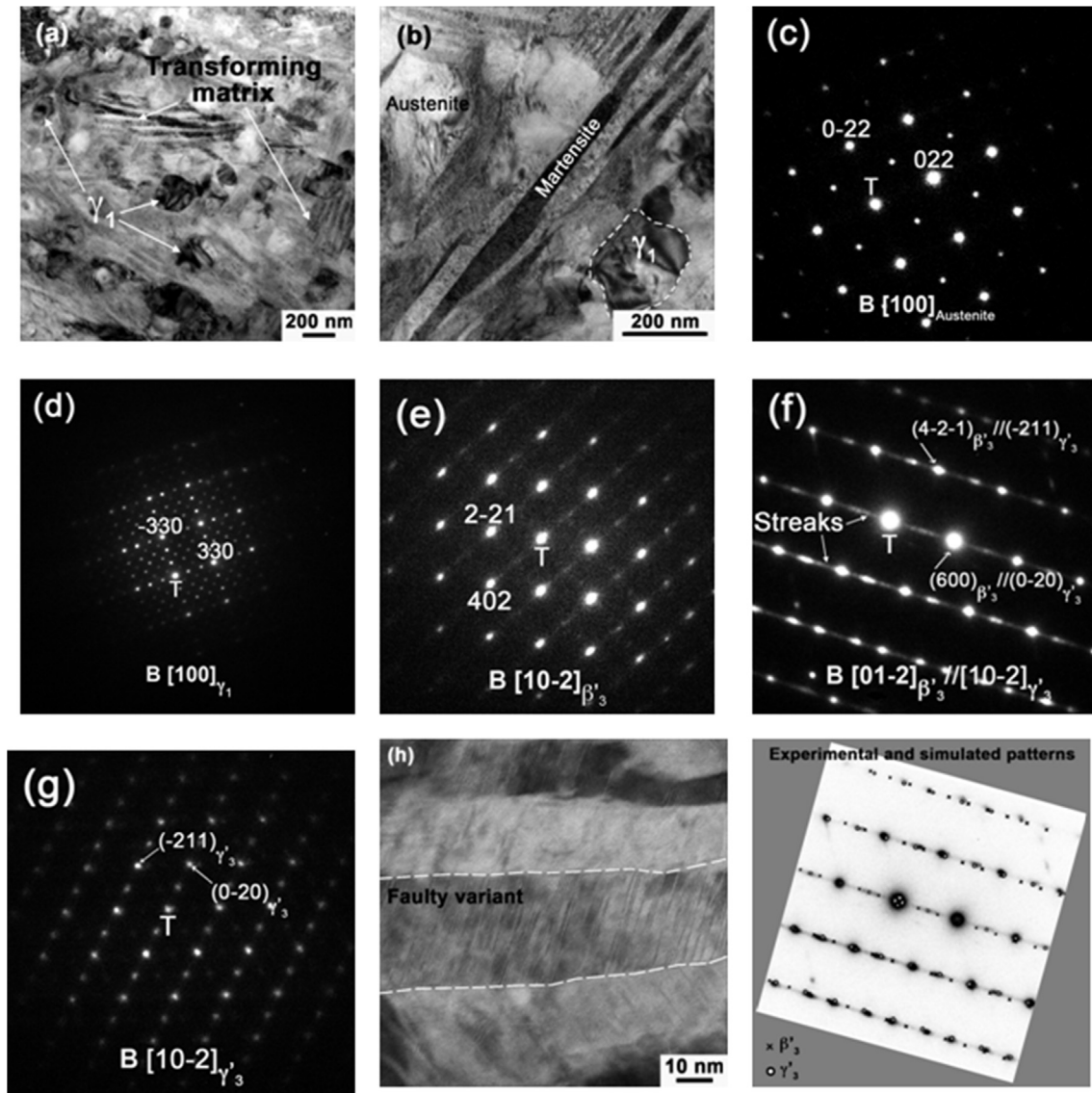


Fig. 3. TEM micrographs of the Cu–14.4 wt% Al–4.3 wt% Ni alloy (B) after HPT. (a) Overview of the duplex microstructure consisting of precipitates of the stable γ_1 homogeneously distributed in a matrix. (b) Enlargement showing the matrix partly transformed into martensite with some areas in austenite state. (c) SAED pattern of an austenite grain. (d) MD pattern of a γ_1 phase precipitate. (e) SAED pattern of β'_3 martensite. (f) MD pattern of β'_3 martensite with streaks along the basal plane and scheme (is shown below the Fig. 3f) of the overlapping the simulated patterns for β'_3 and γ'_3 martensitic phases with an experimental one; crosses and circles correspond to β'_3 martensite and γ'_3 martensite, respectively. (g) MD pattern matching well with that of γ'_3 martensite. (h) Bright field TEM image of the faulty martensites.

domains) of 50 nm after HPT at 4 GPa and 70 nm after HPT at 2 GPa [78]. At a smaller scale, careful TEM investigations of severely deformed pure Cu (HPT, 5 rotations at 7 GPa) permitted to observe grains with size of 100–200 nm containing inside elongated 10–20 nm small subgrains [79]. Taking into account the studies on Cu-based alloys, grain sizes of about 200 nm were also measured for the Cu-rich matrix in Cu–Co, Cu–Ni, Cu–In and Cu–Sn alloys upon HPT processing (3–5 rot, 5–6 GPa) [78,68].

In Fig. 5a a binary section of the ternary Cu–Al–Ni phase diagram constructed on the base of the data of Refs. [65,80] is shown for 3 to 4.5 wt% Ni. The diagram for martensitic transformations in single crystalline samples is shown in Fig. 5b, based on data of Ref. [65]. The same figure (Fig. 5b) also indicates temperatures for austenite start A_s (thin lines) and austenite finish A_f (thick lines) of the reverse transformation, which takes place upon heating from a martensitic state (γ'_3 and/or β'_3 phases) to austenite as a final product. Vertical dashed lines stand for the compositions of the

polycrystalline alloys A and B in both parts of Fig. 5.

On the base of these data, the microstructural evolution under study will now be discussed. Firstly, both studied alloys were homogenized at 900 °C (shown by the full square and circle for alloys A and B, respectively). The correspondent two full symbols are in the one-phase β area of the Cu–Al–Ni phase diagram (Fig. 5a). At the end of the homogenization both samples contain only one phase, namely the disordered β_1 phase ($Im\bar{3}m$ or A_2) with slightly different contents of Al and Ni. The homogenized samples A and B were subsequently quenched in cold water at 0 °C, and, as a consequence of this treatment both alloys (A and B) contain only a solid solution. Upon quenching the diffusion was suppressed and the high-temperature β_1 phase in both samples did not decompose into a mixture of the stable α_1 and γ_1 phases, as predicted by the Cu–Al–Ni phase diagram (Fig. 5a). The respective full square and circle are shown in Fig. 5b at 0 °C. In other words, no precipitation of the stable phases takes place during this quick cooling, and the

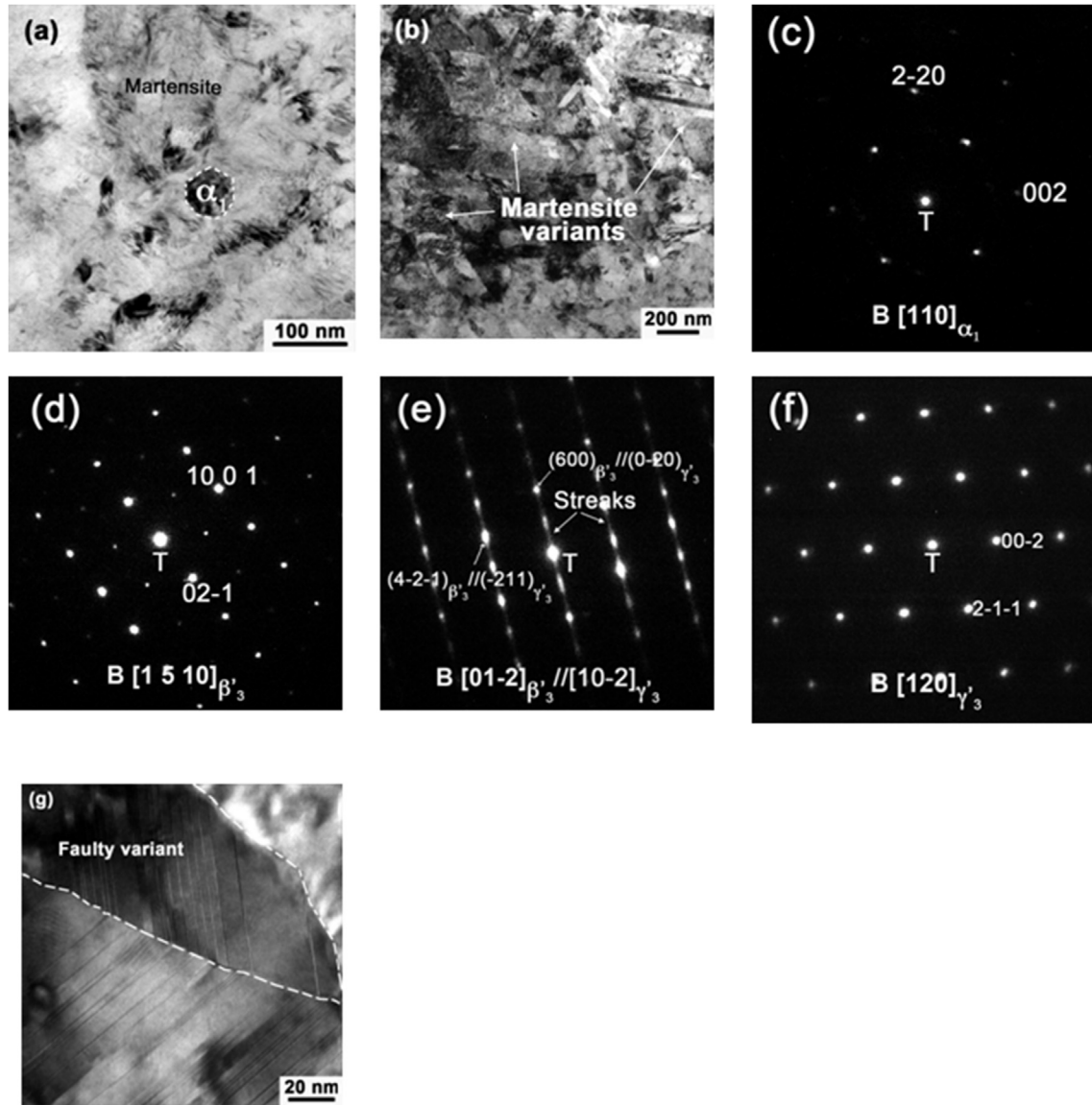


Fig. 4. (a) and (b) TEM micrographs of the Cu–13.1 wt% Al–3.8 wt% Ni alloy (A) after HPT. (c) SAED pattern of the stable α_1 phase. (d) SAED pattern of the β'_3 martensite. (e) MD pattern with streaks along the basal plane of the β'_3 martensite were observed. (f) MD pattern of the γ'_3 martensite obtained by using a very small spot size. (g) Bright field TEM micrograph of the faulty martensites.

composition of the alloys A and B remains uniform. In addition, it is also known that upon quenching the austenite phase undergoes two atomic ordering processes at temperatures higher than the martensitic transformation (lines in Fig. 5b), and consequently the quenched alloys contain the β_3 phase (strongly ordered Fm3m fcc phase with $L2_1$ superstructure and lattice parameter $a = 0.584001$ nm) [82–85], i.e. the ordering processes $\beta_1 \rightarrow \beta_2$ ($B2$) $\rightarrow \beta_3$ ($L2_1$) take place in the β -phase, at least in a partial amount, even upon quick cooling [84].

If no additional thermo-mechanical treatment is applied, instead of the diffusion-controlled eutectoid decomposition $\beta_1 \rightarrow \alpha_1 + \gamma_1$, the strongly ordered β_3 austenite phase would evolve according to martensitic transformations in alloys A and B, when heated/cooled over the transformation temperatures (Fig. 5b). The results of such martensitic phase transformations are different in the hypoeutectoid alloys (as the alloy A) and hypereutectoid alloys (as the alloy B) [65,85,86]. According to the results obtained in single crystalline samples, hypoeutectoid alloys transform into β'_3

martensite while hypereutectoid alloys transform into γ'_3 martensite [56,65]. However, there is a concentration range where both kinds of martensitic phases coexist, i.e. γ'_3 and β'_3 phases (marked in the lower part of Fig. 5b) [56,65]. The martensite evolves from γ'_3 to β'_3 with decreasing Al concentration [56,85,86]. Temperatures of the martensitic reverse transformation for the Cu–Al–Ni alloys are provided as lines in Fig. 5b according to the data of Ref. [56]. The temperatures for forward martensitic transformations, M_s and M_f , are only about 10–20 °C lower and were avoided for the sake of figure simplicity. This transition is metastable and, obviously, does not appear in the stable phase diagram Fig. 5a. According to the phase diagram given in Fig. 5b, the alloys A and B should behave differently after homogenization at 900 °C and quenching in cold water at 0 °C. Namely, on one hand, the β_3 -phase in the alloy A, with a lower Al content, should transform into β'_3 martensite. The filled square at 0 °C is below the lines of martensitic reverse transformation. Consequently, the alloy A contains mainly β'_3 martensite (c.f. Figs. 2 and 4), what in principle is consistent

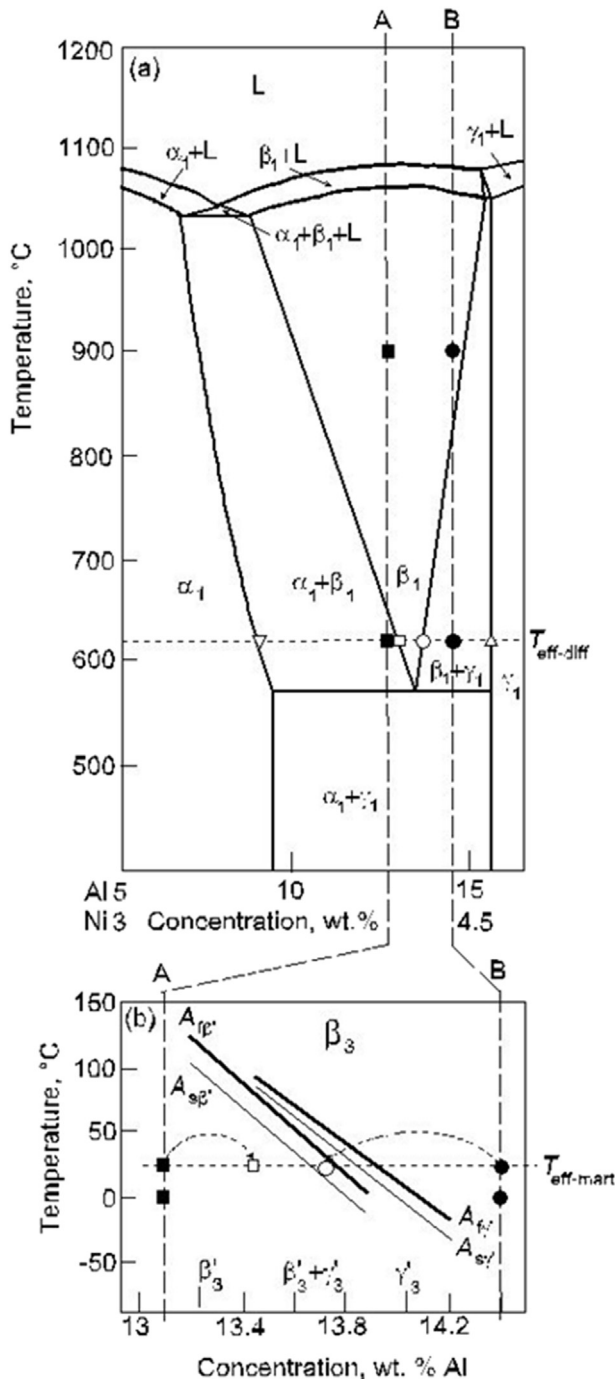


Fig. 5. (a) Binary section of ternary Cu–Ni–Al phase diagram constructed based on the data of Refs. [56,80]. (b) Binary section of ternary Cu–Ni–Al phase diagram with the start A_s (thin lines) and finish A_f (thick lines) temperatures of the reverse transformation from martensite to austenite for γ'_3 and β'_3 phases constructed based on the data of Ref. [56]. Vertical dashed lines show the composition of Alloys A and B. Horizontal dotted lines show the effective temperatures for diffusive $T_{\text{eff-diff}}$ and displacive (martensitic) $T_{\text{eff-mart}}$ transformations. Full symbols show the composition of single-phase solid solution in Alloy A (squares) and Alloy B (circles) after homogenization and before HPT. Open symbols show the composition of martensitic matrix in Alloys A (squares) and B (circles) after HPT. Open triangles show the composition of α -precipitates in the Alloy A (down-triangle) and γ -precipitates in the Alloy B (up-triangle) after HPT. The small grain polycrystalline SMAs exhibit lower transformation temperatures than single crystals, for example in our case the A_f temperatures from Fig. 1d are about 15 °C lower than the corresponding ones for single crystals in Fig. 5b.

with the given reasoning, but the potential influence of the HPT processing has not been taken into account yet. On the other hand, alloy B (filled circle) should remain in austenitic state and contains the ordered β_3 phase (it is the strongly ordered Fm3m fcc phase with L_{21} superstructure and lattice parameter $a = 0.584001$ nm) after quenching (c.f. Figs. 2 and 3). It is worth to mention here that after quenching at 0 °C the samples were not kept in the water-ice mixture, but at a room temperature of about 25 °C, being also the HPT temperature. These points are shown by filled square and circle in Fig. 5b. They are in same phase fields as the points at 0 °C.

Let us discuss now the HPT effect on the investigated samples. It has been already reported that this type of SPD process can drive either diffusive or displacive (diffusionless) phase transformations. Thus, in several Al- and Cu-based alloys the diffusive phase transformations were driven by HPT: namely (a) the decomposition of supersaturated solid solution [7,8,66] or (b) formation of the supersaturated solid solution after partial dissolution of the particles of the second phase in the matrix [8,67]. In Cu–Sn alloys the $\zeta+\epsilon$ phase mixture, present in the as-cast alloy transformed under the action of HPT into the mixture of δ and ϵ phases [68]. Nevertheless, HPT can also induce displacive (martensitic) phase transformations. For example, the low-temperature and low-pressure α -phase in pure Ti and Zr, as well as in Ti- and Zr-based alloys transform under the action of HPT into high-pressure ω -phase or high-pressure and high-temperature β -phase (see Refs. [29,87–93] for works on Ti and Ti-based alloys, and Refs. [94,95] for works on Zr and Zr-based ones). The displacive martensitic transformations proceed without long-distance mass-transfer of the components. However, if the phases appearing in the samples before and after HPT are different from those expected, i.e. the stable α_1 and γ_1 phases occur, one could link the apparition of these phases after HPT to a certain one-phase or two-phase field of the respective equilibrium phase diagram. In other words, HPT induces the formation of phases in such a way, as if the alloy would have been annealed at a certain temperature, what promotes mass transfer. This concept has already been used in the past and the corresponding “annealing” temperature is the so-called effective temperature T_{eff} and it is usually much higher than the temperature of the HPT treatment T_{HPT} [7,9,67,68,96].

In the present case, it is evident that HPT processing has lead to both diffusive and displacive phase transformations. Firstly, the diffusive transformation will be considered. As in other Cu-based alloys [7,8,66,67], and taking into account the observation of the stable α_1 and γ_1 , it can be accepted that HPT has played as an “annealing” at a certain effective temperature T_{eff} . T_{eff} in Cu-based binary alloys increases linearly with increasing activation enthalpy of the diffusion of alloying element [97]. Indeed, HPT has driven a certain mass transfer in the samples treated in this work. To give at least an estimation of such temperature and not pretending to have the highest temperature accuracy, the microstructural information from both samples and the equilibrium phase diagram will be used (Figs. 2–5).

The alloy B was in austenitic state before HPT and contained after quenching only β_3 phase, but after HPT it contained a considerable amount of precipitates of γ_1 phase (c.f. Figs. 2 and 3). The Al content in γ_1 phase is higher than the average Al concentration in the alloy of 14.4 wt% Al. Its composition is shown in Fig. 5a by the open up-triangle. It means that HPT has driven the redistribution of Al atoms from the matrix into the new precipitates of γ_1 phase. As a result, the remaining matrix contained less Al (open circles in Fig. 5a and b) than before HPT (filled circles in Fig. 5a and b). The open circle in Fig. 5a is positioned at the border between one-phase β_1 -area and two-phase $\beta_1+\gamma_1$ area. From the TEM images the weight fraction of the γ_1 phase cannot be quantitatively given, but it can be roughly estimated to be close to 40%. This allows

one to determine the effective temperature at $T_{\text{eff-diff}} \approx 620 \pm 20 \text{ }^\circ\text{C}$ (horizontal dotted line in Fig. 5a). This value must be necessarily consistent with the effective temperature observed for alloy A upon HPT, what is discussed in the following paragraph, because the SPD process was performed under the same conditions on both alloys.

Indeed, in the alloy A few very small precipitates of the stable α_1 phase appeared in the matrix (Fig. 4a). Its composition before HPT is shown by the filled square in the phase diagram Fig. 5a. The filled square is in the $\beta_1 + \alpha_1$ two-phase area but very close to the one-phase β_1 -area, because a very small amount of the α_1 phase was observed. The compositions of the β_1 and α_1 phases in the $\beta_1 + \alpha_1$ two-phase mixture after HPT are shown by the open square and open down-triangle, respectively. Again, from the TEM images the exact weight fraction of the α_1 phase cannot be given, but it can be roughly estimated to be about 4–6%. This is consistent with the effective temperature $T_{\text{eff-diff}} \approx 620 \pm 20 \text{ }^\circ\text{C}$ (horizontal dotted line in Fig. 5a) mentioned in the previous paragraph. The value $T_{\text{eff-diff}}$ cannot be higher than $640 \text{ }^\circ\text{C}$ because the alloy A contains only one phase above $640 \text{ }^\circ\text{C}$. The value $T_{\text{eff-diff}}$ cannot be lower than $600 \text{ }^\circ\text{C}$ because in this case the alloy A would contain enough α_1 phase to be detected by XRD (not only by TEM), what was not the case. Therefore, it can be concluded that both alloys B and A underwent diffusive phase transformation at an effective temperature $T_{\text{eff-diff}} \approx 620 \pm 20 \text{ }^\circ\text{C}$.

This T_{eff} value fits well into the linear dependence between T_{eff} and activation enthalpy of the diffusion of alloying element in different Cu-based alloys [97]. It has to be underlined here that the effective temperature T_{eff} differs from the temperature of HPT experiments T_{HPT} which is about $40\text{--}50 \text{ }^\circ\text{C}$ in our work. In order to substantially change T_{HPT} a special furnace or cooler around the HPT anvils must be used in order to heat or cool them (see for example Ref. [17]), otherwise the temperature remains around the given values. Of course if such special furnace or cooler is used, one also substantially influences the phase transitions in the sample. It is because the relaxation rate in the dynamic equilibrium substantially increases by external heating of the anvils or decreases by their cooling like in Ref. [17].

Secondly, displacive or martensitic transformations will be discussed. They can be explained using the diagram for the forward and reverse martensitic transformations experimentally obtained for single-crystalline Cu–Al–Ni alloys (Fig. 5b) [56]. In the alloy B the β_1 matrix became depleted of Al due to the formation of Al-rich γ_1 -phase precipitates. The matrix composition of the remaining material fraction able to undergo the martensitic transformation, changed from the one shown by the filled circle in Fig. 5a to that shown by the open circle in the same figure. In Fig. 5b this composition shift is shown by the same symbols and arrow. The filled circle is in Fig. 5b in the austenitic area, whereas the Al concentration in the β_3 matrix of the alloy B, after the Al-depletion promoted by SPD, is shifted from the position shown by the filled circle to that shown by the open circle (Fig. 5a). In Fig. 5b this composition shift is indicated by the same symbols and arrow. The open circle in Fig. 5b is in an area where a mixture of β'_3 and γ'_3 martensites exists (together with some remaining β_3 -austenite) according to the data of Ref. [56]. Indeed, our XRD and TEM data witness, that after HPT the matrix contains such mixture of β'_3 and γ'_3 martensites (together with some remaining β_3 -austenite, see Figs. 2 and 3). All these arguments hold only if it is accepted that the “annealing” due to HPT at the so-called effective temperature treated above is subsequently followed by an instantaneous quenching upon stopping the HPT process.

In alloy A the HPT process did not change much the Al-content in the matrix, because the amount of α_1 -phase appearing after HPT is small. For this reason could only be detected in TEM (Fig. 4), but not in the XRD patterns (Fig. 2). The resulted shift from the filled

square to the open square in Fig. 5a is smaller than the shift estimated for the alloy B. The same shift is also shown with the same symbols in Fig. 5b. We observed that before HPT alloy A contained mainly β'_3 martensite, with a small amount of γ'_3 martensite (Fig. 2a). According to the diagram shown in Fig. 5b, only β'_3 martensite should appear, but, although the concentration is the main parameter affecting the type of formed martensite there are others such as grain size or stress level [98,99] that could also have some influence. In fact, small grain polycrystalline SMAs exhibit lower transformation temperatures than single crystals, and this is also verified in our case in which the A_f temperatures from Fig. 1d are about $15 \text{ }^\circ\text{C}$ lower than the corresponding ones for single crystals in Fig. 5b. This is linked to the fact that in polycrystals the nucleation of martensite must produce the lattice shearing against the internal stresses imposed by the grain boundaries. So, the high compressive stress level during the HPT process is undoubtedly one of these parameters affecting the martensitic transformation. In addition, it has been shown [82,99] that in Cu-based SMA, a compressive stress promotes the nucleation of γ'_3 martensite with respect to the β'_3 martensite. In the presented analysis, the data shown in Fig. 5b were determined for single crystalline samples while in the current work polycrystalline samples were used, so, the observed slight discrepancy (a small amount of γ'_3 is present while only β'_3 martensite should have been expected) could be attributed to these secondary parameters affecting the type of appearing martensite. Upon applying HPT on alloy A, again mainly β'_3 martensite was observed (Fig. 4), but in comparison to the sample before HPT a more faulted β'_3 martensite and patterns that fit well with those of the orthorhombic γ'_3 martensite were acquired.

To summarize, we observe in our experiments two effective temperatures. One is called $T_{\text{eff-diff}}$ and describes the phase transformations controlled by the diffusion-like HPT-driven mass transfer. It is higher than the HPT treatment temperature and can be estimated as $T_{\text{eff-diff}} = 620 \pm 20 \text{ }^\circ\text{C}$ (horizontal dotted line in Fig. 5a). During HPT the concentration of components has been changed, as if the alloy would be maintained at $T_{\text{eff-diff}}$. Then the martensitic (displacive, diffusion-less) phase transformations follow this change, taking place as if the material would be quenched from this temperature $T_{\text{eff-diff}}$ down to the temperature of HPT-treatment $T_{\text{eff-HPT}} = 25 \pm 5 \text{ }^\circ\text{C}$ (horizontal dotted line in Fig. 5b) or the effective temperature for the martensitic transformation $T_{\text{eff-mart}} = 25 \pm 5 \text{ }^\circ\text{C}$.

Therefore, HPT drives both kinds of phase transformations: (1) those which need the mass-transfer and redistribution of different atoms on the distances longer than interatomic spacing, and (2) those which do not need the mass-transfer and include only small shifts of atoms on the distances smaller than interatomic spacing. These two simultaneous processes have two different effective temperatures, namely, (1) $T_{\text{eff-diff}} = 620 \pm 20 \text{ }^\circ\text{C}$ and (2) $T_{\text{eff-mart}} = 25 \pm 5 \text{ }^\circ\text{C}$. Thus, it could be said that the changes in austenitic and martensitic phases in both alloys A and B before and after HPT treatment can be well understood as if the alloys were aged at $T_{\text{eff-diff}}$ and then quenched down to $T_{\text{eff-HPT}}$, promoting the diffusionless martensitic phase transformation.

In order to confirm the functionality of the Cu–Al–Ni SMAs, the martensitic transformation behaviour, some DSC measurements were performed and Fig. 6 shows the DSC curves corresponding to Cu–Al–Ni SMA B before and after HPT. As shown above, formation of the stable γ_1 phase occurs and, therefore, the amount of transforming material is reduced, and consequently the heat release (enthalpy) is smaller for the sample after HPT than that for the sample before the severe plastic deformation (pay attention to the scale). In addition, a clear shift of the martensitic transformation temperatures towards higher values together with a strong

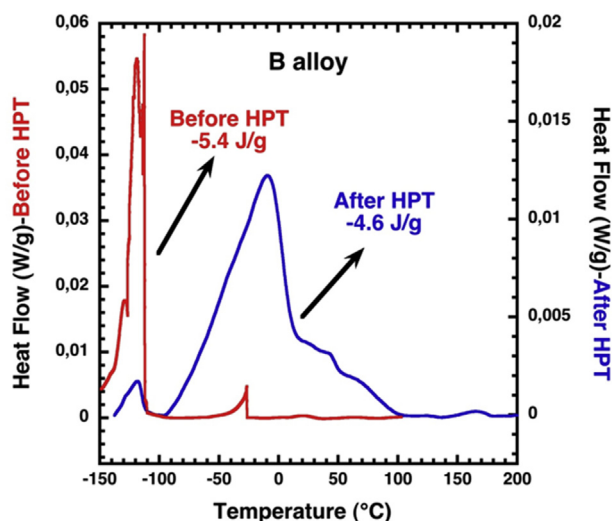


Fig. 6. DSC measurements performed during cooling (forward martensitic transformation) on Cu–Al–Ni SMA B before (red) and after (blue) HPT. A clear shift of the martensitic transformation temperatures towards higher values together with a strong broadening is observed.

broadening is observed. These observations are consistent with discussed composition change and with the large amount of defects introduced by HPT. Anyway, it can be concluded that even by applying an extremely heavy deformation the alloy functionality can be, at least, partly maintained. In other words, it is expected that ultra-fine grained Cu–Al–Ni SMAs with improved mechanical and functional properties can be produced by HPT. This is an outstanding point, because Cu–Al–Ni SMAs do not support cold-rolling for grain refinement (they are very brittle at low temperature) and during hot-rolling the grain growth by dynamic recrystallization. Thus, HPT processing could be seen as the only one method allowing a good refinement of the grain size, and consequently an exceptional method to improve the thermo-mechanical and functional properties of polycrystalline Cu–Al–Ni SMA.

Finally, let us estimate the rate of mass transfer during HPT. In both alloys the average distance between precipitates formed during HPT from the partially transformed matrix is about 100 nm. The approximate relationship $L \approx (D_{\text{HPT}}t)^{0.5}$ ($t = 300$ s being the HPT treatment duration) yields $D_{\text{HPT}} = 3 \times 10^{-17}$ m²/s. It is considered here that it is unlikely that bulk interdiffusion is responsible for decomposition during the HPT processing. Indeed, the range of bulk chemical interdiffusion coefficients in Cu–Al and Cu–Ni alloys at room temperature can be estimated by impurity diffusion coefficients of Al in Cu, $D_{\text{Cu}}^{\text{Al}}$, and Ni in Cu, $D_{\text{Cu}}^{\text{Ni}}$. Extrapolating the literature data to the room temperature (25 °C) yields $D_{\text{Cu}}^{\text{Al}} = 5 \times 10^{-37}$ m²/s [100,101], and $D_{\text{Cu}}^{\text{Ni}} = 4.8 \times 10^{-44}$ m²/s [100,102]. The diffusion data also exist for the binary Cu–Al β intermetallic phase, which is the most similar to our alloy [103]. Extrapolating them down to room temperature we get: $D_{\beta}^{\text{Al}} = 3.8 \times 10^{-34}$ m²/s, $D_{\beta}^{\text{Cu}} = 3.8 \times 10^{-36}$ m²/s, and $\bar{D} = 7.3 \times 10^{-36}$ m²/s. These values are larger than the values we estimated for a solid solution, and closer to the estimated value of D_{HPT} .

These diffusivities can be significantly increased by the non-equilibrium excess vacancies produced during HPT. Assuming that the highest vacancy concentration that a solid can sustain corresponds to the equilibrium vacancy concentration at the melting temperature, and with literature values of vacancy formation enthalpy of 1.28 eV for Cu [104], we estimate the maximal room temperature diffusivity as $D_{\text{Cu}}^{\text{Ni}} = 3 \times 10^{-27}$ m²/s. This value is

still 10 orders of magnitude lower than our estimate $D = 3 \times 10^{-17}$ m²/s. This means that the external pressure can additionally slow down the diffusion [105,106]. At the same time, extrapolating the diffusion coefficients along the “ultrafast” GBs measured recently in the pure Ni [107] and Cu–Zr alloy [108] processed by equal channel angular pressing (ECAP) yields the room temperature GB diffusivities in the range of 3×10^{-20} m²/s. This is closer to our estimate of $D = 3 \times 10^{-17}$ m²/s, with the remaining difference of three orders of magnitude that can be possibly associated with the uncertainties in determining D , the differences between the ECAP and HPT processes, as well as with the fact that diffusion measurements in Refs. [107,109] were performed after the ECAP process, so that a significant part of non-equilibrium defects had a time to annihilate. In conclusion, simple estimates presented above lend credibility to the hypothesis that the GB, rather than bulk interdiffusion controls the decomposition process both in alloys A and B. Thus, the mass transfer during HPT (namely, partial decomposition of alloys A and B) proceeds very quick. This fact correlates with our previous observations on the extremely high rate of mass transfer and diffusion-controlled phase transformations in the Al–Zn [66], Cu–Ni [7], Cu–Co [7,9], Cu–In Ref. [67] and Cu–Sn [68] alloys during HPT. However, the simultaneous diffusive and displacive phase transformations driven by HPT are observed in this work for the first time.

5. Conclusions and perspectives

In conclusion, the obtained results show that high-pressure torsion applied to Cu–Al–Ni shape memory alloys in both austenitic (β_3) and martensitic ($\beta'_3 + \gamma'_3$) states leads to a strong grain refinement and to the transitions into the β'_3 martensite (with small amount of γ'_3 martensite). This can be explained by the HPT-driven decomposition of both alloys (as if they would be annealed at $T_{\text{eff-diff}} = 620 \pm 20$ °C) and a subsequent quenching down to $T_{\text{eff-HPT}} = 25 \pm 5$ °C that promotes the diffusionless martensitic phase transformations. This severe plastic deformation methodology opens the way for the production of nanostructured Cu-based SMA with tailored microstructure and properties.

Acknowledgments

The work was partially supported by the Russian Foundation for Basic Research (grants 15-08-09325, 16-53-12007 and 14-48-03598), Deutsche Forschungsgemeinschaft, Government of Moscow Region, the Russian Federal Ministry for Education and Science under Increase Competitiveness Program of NUST«MISIS» for the financial support, and Karlsruhe Nano Micro Facility. The authors thank the Spanish Ministry of Economy and Competitiveness, MINECO, project MAT2012-36421 and the CONSOLIDER-INGENIO CSD2009-00013, as well as the Consolidated Research Group IT-10-310 and the ELKARTEK-ACTIMAT-2015 from the Basque Government.

References

- [1] X. Sauvage, A. Chbihi, X. Quelehenec, Severe plastic deformation and phase transformations, *J. Phys.* 240 (2010) 012003.
- [2] W. Lojkowski, M. Djahanbakhsh, G. Burkle, S. Gierlotka, W. Zielinski, H.J. Fecht, Nanostructure formation on the surface of railway tracks, *Mater. Sci. Eng. A* 303 (2001) 197–208.
- [3] V.G. Gavriljuk, Decomposition of cementite in pearlitic steel due to plastic deformation, *Mater. Sci. Eng. A* 345 (2003) 81–89.
- [4] X. Sauvage, F. Wetscher, P. Pareige, Mechanical alloying of Cu and Fe induced by severe plastic deformation of a Cu–Fe composite, *Acta Mater.* 53 (2005) 2127–2135.
- [5] B.B. Straumal, B. Baretzky, A.A. Mazilkin, F. Phillipp, O.A. Kogtenkova,

- M.N. Volkov, R.Z. Valiev, Formation of nanograin structure and decomposition of supersaturated solid solution during high pressure torsion of Al–Zn and Al–Mg, *Acta Mater.* 52 (2004) 4469–4478.
- [6] A.A. Mazilkin, B.B. Straumal, E. Rabkin, B. Baretzky, S. Enders, S.G. Protasova, O.A. Kogtenkova, R.Z. Valiev, Softening of nanostructured Al–Zn and Al–Mg alloys after severe plastic deformation, *Acta Mater.* 54 (2006) 3933–3939.
- [7] B.B. Straumal, S.G. Protasova, A.A. Mazilkin, E. Rabkin, D. Goll, G. Schütz, B. Baretzky, R. Valiev, Deformation-driven formation of equilibrium phases in the Cu–Ni alloys, *J. Mater. Sci.* 47 (2012) 360–367.
- [8] B.B. Straumal, A.R. Kilmametov, Yu.O. Kucheev, L. Kurmanaeva, Yu. Ivanisenko, B. Baretzky, A. Korneva, P. Zięba, D.A. Molodov, Phase transitions during high pressure torsion of Cu–Co alloys, *Mater. Lett.* 118 (2014) 111–114.
- [9] B.B. Straumal, A.A. Mazilkin, B. Baretzky, E. Rabkin, R.Z. Valiev, Accelerated diffusion and phase transformations in Co–Cu alloys driven by the severe plastic deformation, *Mater. Trans.* 53 (2012) 63–71.
- [10] C.M. Cepeda-Jiménez, J.M. García-Infanta, A.P. Zhilyaev, O.A. Ruano, F. Carreño, Influence of the thermal treatment on the deformation-induced precipitation of a hypoeutectic Al–7 wt% Si casting alloy deformed by high-pressure torsion, *J. Alloys Comp.* 509 (2011) 636–643.
- [11] Y. Ivanisenko, W. Lojkowski, R.Z. Valiev, H.J. Fecht, The mechanism of formation of nanostructure and dissolution of cementite in a pearlitic steel during high pressure torsion, *Acta Mater.* 51 (2003) 5555–5570.
- [12] B.B. Straumal, A.A. Mazilkin, S.G. Protasova, S.V. Dobatkin, A.O. Rodin, B. Baretzky, D. Goll, G. Schütz, Fe–C nanograin alloys obtained by high pressure torsion: structure and magnetic properties, *Mater. Sci. Eng. A* 503 (2009) 185–189.
- [13] V.V. Sagaradze, V.A. Shabashov, Deformation-induced anomalous phase transformations in nanocrystalline FCC Fe–Ni based alloys, *Nanostruct. Mater.* 9 (1997) 681–684.
- [14] S. Ohsaki, S. Kato, N. Tsuji, T. Ohkubo, K. Hono, Bulk mechanical alloying of Cu–Ag and Cu/Zr two-phase microstructures by accumulative roll-bonding process, *Acta Mater.* 55 (2007) 2885–2895.
- [15] B.B. Straumal, S.V. Dobatkin, A.O. Rodin, S.G. Protasova, A.A. Mazilkin, D. Goll, B. Baretzky, Structure and properties of nanograin Fe–C alloys after severe plastic deformation, *Adv. Eng. Mater.* 13 (2011) 463–469.
- [16] A.V. Sergueeva, C. Song, R.Z. Valiev, A.K. Mukherjee, Structure and properties of amorphous and nanocrystalline NiTi prepared by severe plastic deformation and annealing, *Mater. Sci. Eng. A* 339 (2003) 159–165.
- [17] S.D. Prokoshkin, I.Yu. Khmelevskaya, S.V. Dobatkin, I.B. Trubitsyna, E.V. Tatyani, V.V. Stolyarov, E.A. Prokofiev, Alloy composition, deformation temperature, pressure and post-deformation annealing effects in severely deformed Ti–Ni based shape memory alloys, *Acta Mater.* 53 (2005) 2703–2714.
- [18] X. Sauvage, L. Renaud, B. Deconihout, D. Blavette, D.H. Ping, K. Hono, Solid state amorphization in cold drawn Cu/Nb wires, *Acta Mater.* 49 (2001) 389–394.
- [19] T. Miyazaki, D. Terada, Y. Miyajima, C. Suryanarayana, R. Mura, Y. Yokoyama, K. Sugiyama, M. Umamoto, T. Todaka, N. Tsuji, Synthesis of non-equilibrium phases in immiscible metals mechanically mixed by high pressure torsion, *J. Mater. Sci.* 46 (2011) 4296–4301.
- [20] A.A. Mazilkin, G.E. Abrosimova, S.G. Protasova, B.B. Straumal, G. Schütz, S.V. Dobatkin, A.S. Bakai, Transmission electron microscopy investigation of boundaries between amorphous “grains” in Ni₅₀Nb₂₀Y₃₀ alloy, *J. Mater. Sci.* 46 (2011) 4336–4342.
- [21] B.B. Straumal, A.A. Mazilkin, S.G. Protasova, D. Goll, B. Baretzky, A.S. Bakai, S.V. Dobatkin, Formation of two amorphous phases in the Ni₅₀Nb₁₈Y₂₂ alloy after high pressure torsion, *Kovove Mater. Metall. Mater.* 49 (2011) 17–22.
- [22] A.M. Glezer, M.R. Plotnikov, A.V. Shalimova, S.V. Dobatkin, Severe plastic deformation of amorphous alloys: I. Structure and mechanical properties, *Bull. Russ. Ac. Sci. Phys.* 73 (2009) 1233–1236.
- [23] G.E. Abrosimova, A.S. Aronin, S.V. Dobatkin, S.D. Kaloshkin, D.V. Matveev, G.G. Rybchenko, E.V. Tatyani, I.I. Zverkova, The formation of nanocrystalline structure in amorphous Fe–Si–B alloy by severe plastic deformation, *J. Metastab. Nanocryst. Mater.* 24 (2005) 69–72.
- [24] P. Henits, Á. Révész, A.P. Zhilyaev, Zs. Kovács, Severe plastic deformation induced nanocrystallization of melt-spun Al₈₅Y₈Ni₅Co₂ amorphous alloy, *J. Alloys Comp.* 461 (2008) 195–199.
- [25] B.B. Straumal, V. Pontikis, A.R. Kilmametov, A.A. Mazilkin, S.V. Dobatkin, B. Baretzky, Competition between precipitation and dissolution in Cu–Ag alloys under high pressure torsion, *Acta Mater.* 122 (2017) 60–71.
- [26] C.X. Huang, G. Yang, Y.L. Gao, S.D. Wu, S.X. Li, Investigation on the nucleation mechanism of deformation-induced martensite in an austenitic stainless steel under severe plastic deformation, *J. Mater. Res.* 22 (2007) 724–729.
- [27] T. Waitz, W. Pranger, T. Antretter, F.D. Fischer, H.P. Karnthaler, Competing accommodation mechanisms of the martensite in nanocrystalline NiTi shape memory alloys, *Mater. Sci. Eng. A* 481–482 (2008) 479–483.
- [28] S. Jiang, Y. Zhang, L. Zhao, Y. Zheng, Influence of annealing on NiTi shape memory alloy subjected to severe plastic deformation, *Intermetallics* 32 (2013) 344–351.
- [29] Yu. Ivanisenko, A. Kilmametov, H. Roesner, R.Z. Valiev, Evidence of $\alpha \rightarrow \omega$ phase transition in titanium after high pressure torsion, *Int. J. Mater. Res.* 99 (2008) 36–41.
- [30] A.R. Pelton, D. Hodgson, T.W. Duering (Eds.), *Shape Memory and Superelastic Technologies*, Proc. SMST-94, MIAS, Asilomar, Monterey CA, 1995.
- [31] L. Delaey, Diffusionless transformations, in: P. Haasen (Ed.), *Phase Transformations in Materials*, VCH, Weinheim, Germany, 1991, pp. 339–404.
- [32] K. Otsuka, C.M. Wayman (Eds.), *Shape Memory Materials*, Cambridge University Press, Cambridge, 1999.
- [33] K. Otsuka, X. Ren, Physical metallurgy of Ti–Ni-based shape memory alloys, *Prog. Mater. Sci.* 50 (2005) 511–678.
- [34] Y. Yamauchi, I. Ohkata, K. Tsuchiya, S. Miyazaki (Eds.), *Shape Memory and Superelastic Alloys*, Woodhead Publishing, Cambridge, 2009.
- [35] L. Sun, W.M. Huang, Z. Ding, Y. Zhao, C.C. Wang, H. Purnawali, C. Tang, Stimulus-responsive shape memory materials: a review, *Mater. Des.* 33 (2012) 577–640.
- [36] J.M. Jani, M. Leary, A. Subic, M.A. Gibson, A review of shape memory alloy research, applications and opportunities, *Mater. Des.* 56 (2014) 1078–1113.
- [37] A. Ziolkowski, *Pseudoelasticity of Shape Memory Alloys; Theory and Experimental Studies*, Butterworth-Heinemann, Oxford, 2015.
- [38] T. Yonemaya, S. Miyazaki (Eds.), *Shape Memory Alloys for Biomedical Applications*, Woodhead Publishing, Cambridge, 2009.
- [39] M. Niinomi, M. Nakai, J. Hieda, Development of new metallic alloys for biomedical applications, *Acta Biomater.* 8 (2012) 3888–3903.
- [40] C. Lagoudas (Ed.), *Shape Memory Alloys; Modeling and Engineering Applications*, Springer, New York, 2008.
- [41] O. Kastner, *First Principles Modelling of Shape Memory Alloys; Molecular Dynamics Simulations*, Springer, New York, 2012.
- [42] M. Kohl, *Shape Memory Microactuators*, Springer, New York, 2004.
- [43] Y. Fu, H. Du, W. Huang, S. Zhang, M. Hu, TiNi-based thin films in MEMS applications: a review, *Sens. Actuat. A Phys.* 112 (2004) 395–408.
- [44] S. Miyazaki, Y.Q. Fu, W.M. Huang, *Shape Memory Thin Films*, Cambridge University Press, Cambridge, 2009.
- [45] J. San Juan, M.L. Nó, C.A. Schuh, Superelasticity and shape memory in micro- and nanometer-scale pillars, *Adv. Mater.* 20 (2008) 272–278.
- [46] J. San Juan, M.L. Nó, C.A. Schuh, Nanoscale shape-memory alloys for ultrahigh mechanical damping, *Nat. Nanotech.* 4 (2009) 415–419.
- [47] J. San Juan, J.F. Gómez-Cortés, G.A. López, C. Jiao, M.L. Nó, *Appl. Phys. Lett.* 104 (2014) 011901.
- [48] A. Creuziger, W.C. Crone, Grain boundary fracture in CuAlNi shape memory alloys, *Mater. Sci. Eng. A* 498 (2008) 404–411.
- [49] J.V. Wood, P.H. Shingu, The effect of processing conditions and subsequent heat treatment on the transformation behavior of some rapidly solidified copper-base shape memory alloys, *Metall. Trans. A* 15 (1984) 471–480.
- [50] J.S. Lee, C.M. Wayman, Grain refinement of a Cu–Al–Ni shape memory alloy by Ti and Zr additions, *T. Jpn. I. Met.* 27 (1986) 584–591.
- [51] V. Sampath, Studies on the effect of grain refinement and thermal processing on shape memory characteristics of Cu–Al–Ni alloys, *Smart Mater. Struct.* 14 (2005) S253–S260.
- [52] A. Ibarra, J. San Juan, E.H. Bocanegra, M.L. Nó, Thermo-mechanical characterization of Cu–Al–Ni shape memory alloys elaborated by powder metallurgy, *Mater. Sci. Eng. A* 438–440 (2008) 782–786.
- [53] S.K. Vajpai, R.K. Dube, P. Chatterjee, S. Sangal, A novel powder metallurgy processing approach to prepare fine-grained Cu–Al–Ni shape-memory alloy strips from elemental powders, *Metall. Mater. Trans. A* 43 (2012) 2484–2499.
- [54] J. San Juan, R.B. Pérez-Sáez, V. Recarte, M.L. Nó, G. Caruana, M. Lieblich, O. Ruano, Martensitic Transformation in Cu–Al–Ni shape memory alloys processed by powder metallurgy, *J. Phys. IV* 05 (1995), C8–919–C8–924.
- [55] R.B. Pérez-Sáez, V. Recarte, M.L. Nó, O.A. Ruano, J. San Juan, Advanced shape memory alloys processed by powder metallurgy, *Adv. Eng. Mater.* 2 (2000) 49–53.
- [56] V. Recarte, R.B. Pérez-Sáez, E.H. Bocanegra, M.L. No, J. San Juan, Influence of Al and Ni concentration on the martensitic transformation in Cu–Al–Ni shape-memory alloys, *Metall. Mater. Trans. A* 33 (2002) 2581–2591.
- [57] M.J. Zehetbauer, R.Z. Valiev (Eds.), *Nanomaterials by Severe Plastic Deformation Hardcover*, Wiley-VCH, Weinheim, 2004.
- [58] R.Z. Valiev, R.K. Islamgaliev, I.V. Alexandrov, Bulk nanostructured materials from severe plastic deformation, *Prog. Mater. Sci.* 45 (2000) 103–189.
- [59] V.M. Segal, I.J. Beyerlein, C.N. Tome, V.N. Chuvil'deev, V.I. Kopylov, *Fundamentals and Engineering of Severe Plastic Deformation*, Nova Science Publishers, New York, 2011.
- [60] R.Z. Valiev, A.P. Zhilyaev, T. Langdon, *Bulk Nanostructured Materials: Fundamentals and Applications*, Wiley, Hoboken, 2013.
- [61] Y.T. Zhu, V. Varyukhin, *Nanostructured Materials by High-pressure Severe Plastic Deformation*, Springer, Dordrecht, 2004.
- [62] D.V. Gunderov, V.Yu. Slesarenko, A.A. Churakova, A.V. Lukyanov, E.P. Soshnikova, V.G. Pushin, R.Z. Valiev, Evolution of the amorphous structure in melt-spun Ti₅₀Ni₂₅Cu₂₅ alloy subjected to high pressure torsion deformation, *Intermetallics* 66 (2015) 77–81.
- [63] R.Z. Valiev, D.V. Gunderov, A.V. Lukyanov, V.G. Pushin, Mechanical behavior of nanocrystalline TiNi alloy produced by severe plastic deformation, *J. Mater. Sci.* 47 (2012) 7848–7853.
- [64] E. Prokofiev, J. Burrow, J. Frenzel, D. Gunderov, G. Eggeler, R. Valiev, Phase transformations and functional properties of NiTi alloy with ultrafine-grained structure, *Mater. Sci. Forum* 667–669 (2011) 1059–1064.
- [65] V. Recarte, R.B. Pérez-Sáez, E.H. Bocanegra, M.L. No, J. San Juan, Dependence of the martensitic transformation characteristics on concentration in Cu–Al–Ni shape memory alloys, *Mater. Sci. Eng. A* 273–275 (1999) 380–384.
- [66] B. Straumal, R. Valiev, O. Kogtenkova, P. Zieba, T. Czepe, E. Bielanska,

- M. Faryna, Thermal evolution and grain boundary phase transformations in severe deformed nanograined Al–Zn alloys, *Acta Mater.* 56 (2008) 6123–6131.
- [67] B.B. Straumal, A.R. Kilmametov, A.A. Mazilkin, L. Kurmanaeva, Y. Ivanisenko, A. Korneva, P. Zięba, B. Baretzky, Transformations of Cu(In) supersaturated solid solutions under high-pressure torsion, *Mater. Lett.* 138 (2015) 255–258.
- [68] B.B. Straumal, A.R. Kilmametov, Yu. O. Kucheev, K.I. Kolesnikova, A. Korneva, P. Zięba, B. Baretzky, Transformations of Hume-Rothery phases under the action of high pressure torsion, *JETP Lett.* 100 (2014) 376–379.
- [69] B.B. Straumal, A.R. Kilmametov, Yu. Ivanisenko, A.A. Mazilkin, O.A. Kogtenkova, L. Kurmanaeva, A. Korneva, P. Zięba, B. Baretzky, Phase transitions induced by severe plastic deformation: steady-state and equifinality, *Int. J. Mater. Res.* 106 (2015) 657–664.
- [70] J. Markmann, V. Yamakov, J. Weissmueller, Validating grain size analysis from X-ray line broadening: a virtual experiment, *Scr. Mater.* 59 (2008) 15–18.
- [71] M. Wojdyr, Fityk: a general-purpose peak fitting program, *J. Appl. Cryst.* 43 (2010) 1126–1128.
- [72] V. Recarte, I. Hurtado, J. Herreros, M.L. Nó, J. San Juan, Precipitation of the stable phases in Cu–Al–Ni shape memory alloys, *Scr. Mater.* 34 (1996) 255–260.
- [73] J.I. Pérez-Landazábal, V. Recarte, V. Sánchez-Alarcos, M.L. Nó, J. San Juan, Study of the stability and decomposition process of the β phase in Cu–Al–Ni shape memory alloys, *Mater. Sci. Eng. A* 438–440 (2006) 734–737.
- [74] A. Ibarra, J. San Juan, E.H. Bocanegra, D. Caillard, M.L. Nó, “In situ” and “Post-mortem” TEM study of the super-elastic effect in Cu–Al–Ni shape memory alloys, *Mater. Sci. Eng. A* 438–440 (2006) 787–790.
- [75] J. Ye, M. Tokonami, K. Otsuka, Crystal structure analysis of γ' Cu–Al–Ni martensite using conventional X-rays and synchrotron radiations, *Metall. Trans. A* 21 (1990) 2669–2678.
- [76] J.I. Pérez-Landazábal, V. Recarte, R.B. Pérez-Sáez, M.L. Nó, J. Campo, J. San Juan, Determination of the next-nearest neighbor order in β phase in Cu–Al–Ni shape memory alloys, *Appl. Phys. Lett.* 81 (2002) 1794–1796.
- [77] N. Lugo, N. Llorca, J.M. Cabrera, Z. Horita, Microstructures and mechanical properties of pure copper deformed severely by equal-channel angular pressing and high pressure torsion, *Mater. Sci. Eng. A* 477 (2008) 366–371.
- [78] J. Čížek, M. Janeček, O. Srba, R. Kuzel, Z. Barnovska, I. Prochazka, S. Dobatkin, Evolution of defects in copper deformed by high-pressure torsion, *Acta Mater.* 59 (2011) 2322–2329.
- [79] X.Z. Liao, Y.H. Zhao, Y.T. Zhu, R.Z. Valiev, D.V. Gunderov, Grain-size effect on the deformation mechanisms of nanostructured copper processed by high-pressure torsion, *J. Appl. Phys.* 96 (2004) 636–640.
- [80] Y.S. Sun, G.W. Lorimer, N. Ridley, Microstructure and its development in Cu–Al–Ni alloys, *Metall. Trans. A* 21 (1990) 575–588.
- [81] M.L. Nó, A. Ibarra, D. Caillard, J. San Juan, Quantitative analysis of stress-induced martensites by in situ transmission electron microscopy superelastic tests in Cu–Al–Ni shape memory alloys, *Acta Mater.* 52 (2010) 6181–6193.
- [82] V. Novak, P. Sittner, Stability of γ' martensite in Cu-base alloys, *J. Phys. IV Fr.* 7 (1997), C5-227–C5-332.
- [83] V. Recarte, O.A. Lambri, R.B. Pérez-Sáez, M.L. Nó, J. San Juan, Ordering temperatures in Cu–Al–Ni shape memory alloys, *Appl. Phys. Lett.* 70 (1997) 3513–3515.
- [84] V. Recarte, R.B. Pérez-Sáez, M.L. Nó, J. San Juan, Ordering kinetics in Cu–Al–Ni shape memory alloys, *J. Appl. Phys.* 86 (1999) 5467–5473.
- [85] A.Y. Vasilenko, V.A. Sal'nikov, A.T. Kosilov, Internal friction in loaded single crystals of Cu–Al–Ni, *Phys. Met. Metallogr.* 4 (1982) 694–697.
- [86] C.M. Friend, The effect of aluminium content on the martensite phase stabilities in metastable CuAlNi alloys, *Scr. Metall.* 23 (1989) 1817–1820.
- [87] K. Edalati, E. Matsubara, Z. Horita, Processing pure Ti by high-pressure torsion in wide ranges of pressures and strain, *Metall. Mater. Trans. A* 40 (2009) 2079–2086.
- [88] R.K. Islamgaliev, V.U. Kazhyhanov, L.O. Shestakova, A.V. Sharafutdinov, R.Z. Valiev, Microstructure and mechanical properties of titanium (Grade 4) processed by high-pressure torsion, *Mater. Sci. Eng. A* 493 (2008) 190–194.
- [89] A.V. Sergueeva, V.V. Stolyarov, R.Z. Valiev, A.K. Mukherjee, Advanced mechanical properties of pure titanium with ultrafine grained structure, *Scr. Mater.* 45 (2001) 747–752.
- [90] R.Z. Valiev, A.V. Sergueeva, A.K. Mukherjee, The effect of annealing on tensile deformation behavior of nanostructured SPD titanium, *Scr. Mater.* 49 (2003) 669–674.
- [91] I. Todaka, J. Sasaki, T. Moto, M. Umamoto, Bulk submicrocrystalline ω -Ti produced by high-pressure torsion straining, *Scr. Mater.* 59 (2008) 615–618.
- [92] I. Todaka, M. Umamoto, A. Yamazaki, J. Sasaki, K. Tsuchiya, Effect of strain path in high-pressure torsion process on hardening in commercial purity titanium, *Mater. Trans.* 49 (2008) 47–53.
- [93] B.B. Straumal, A.R. Kilmametov, Yu. Ivanisenko, A.S. Gornakova, A.A. Mazilkin, M.J. Kriegl, O.B. Fabrichnaya, B. Baretzky, H. Hahn, Phase transformations in Ti–Fe alloys induced by high pressure torsion, *Adv. Eng. Mater.* 17 (2015) 1835–1841.
- [94] K. Edalati, Z. Horita, Y. Mine, High-pressure torsion of hafnium, *Mater. Sci. Eng. A* 527 (2010) 2136–2141.
- [95] A.P. Zhilyaev, I. Sabirov, G. González-Doncela, J. Molina-Aldareguía, B. Srinivasarao, M.T. Pérez-Prado, Effect of Nb additions on the microstructure, thermal stability and mechanical behavior of high pressure Zr phases under ambient conditions, *Mater. Sci. Eng. A* 528 (2011) 3496–3505.
- [96] B. Straumal, A. Korneva, P. Zięba, Phase transitions in metallic alloys driven by the high pressure torsion, *Arch. Civ. Mech. Eng.* 14 (2014) 242–249.
- [97] B.B. Straumal, A.R. Kilmametov, A. Korneva, A.A. Mazilkin, P.B. Straumal, P. Zięba, B. Baretzky, Phase transitions in Cu-based alloys under high pressure torsion, *J. Alloys Comp.* (2017) in press.
- [98] K. Mukunthan, L.C. Brown, Preparation and properties of fine grain β -CuAlNi strain-memory alloys, *Metall. Trans. A* 19 (1988) 2921–2929.
- [99] P. Sittner, V. Novak, Anisotropy of martensitic transformations in modeling of shape memory alloy polycrystals, *Int. J. Plast.* 16 (2000) 1243–1268.
- [100] H. Mehrer (Ed.), *Diffusion in Solid Metals and Alloys*, Landolt-börnstein New Series, Gr III, vol. 26, Springer-Verlag, Berlin, 1990.
- [101] R.L. Fogelson, Ya.A. Ugay, A.V. Pokoyev, Bulk diffusion of aluminium in copper, *Izv. Vyssh. Uchebn. Zaved. Tsvetn. Metall.* 16 (1973) 143–148 (in Russian).
- [102] C.A. Macklitt, Diffusion of iron, cobalt, and nickel in single crystals of pure copper, *Phys. Rev.* 109 (1958) 1964–1968.
- [103] A.D. Romig Jr., Interdiffusion in β phase Cu–Al alloys, *J. Appl. Phys.* 54 (1983) 3172–3175.
- [104] H.-E. Schaefer, Investigation of thermal equilibrium vacancies in metals by positron annihilation, *Phys. Stat. Sol. A* 102 (1987) 47–65.
- [105] B.B. Straumal, L.M. Klinger, L.S. Shvindlerman, The influence of pressure on indium diffusion along single tin–germanium interphase boundaries, *Scr. Metall.* 17 (1983) 275–279.
- [106] D.A. Molodov, B.B. Straumal, L.S. Shvindlerman, The effect of pressure on migration of the [001] tilt grain boundaries in the tin bicrystals, *Scr. Metall.* 18 (1984) 207–211.
- [107] S.V. Divinski, G. Reglitz, H. Rösner, Y. Estrin, G. Wilde, Ultra-fast diffusion channels in pure Ni severely deformed by equal-channel angular pressing, *Acta Mater.* 59 (2011) 1974–1985.
- [108] Y. Amouyal, S.V. Divinski, Y. Estrin, E. Rabkin, Short-circuit diffusion in an ultrafine-grained copper-zirconium alloy produced by equal channel angular pressing, *Acta Mater.* 55 (2007) 5968–5979.
- [109] P. Bellon, R.S. Averbach, Nonequilibrium roughening of interfaces in crystals under shear: application to ball milling, *Phys. Rev. Lett.* 74 (1995) 1819–1822.